remote sensing

MDPI

Technical Note

Aerosol Direct Radiative Effects under Cloud-Free Conditions over Highly-Polluted Areas in Europe and Mediterranean: A Ten-Years Analysis (2007–2016)

Tony C. Landi [1], Paolo Bonasoni [1], Michele Brunetti [1], James R. Campbell [2], Jared W. Marquis [3], Paolo Di Girolamo [4] and Simone Lolli [5,6,*]

1 CNR-ISAC, Via Gobetti 101, 40129 Bologna, Italy; t.landi@isac.cnr.it (T.C.L.); p.bonasoni@isac.cnr.it (P.B.); m.brunetti@isac.cnr.it (M.B.)
2 Naval Research Laboratory, Monterey, CA 93940, USA; james.campbell@nrlmry.navy.mil
3 Department of Atmospheric Sciences, University of North Dakota, Grand Forks, ND 58202, USA; jared.marquis@und.edu
4 Scuola di Ingegneria, Università degli Studi della Basilicata, 85100 Potenza, Italy; paolo.digirolamo@unibas.it
5 CNR-IMAA, Contrada S. Loja, s.n.c, 85050 Tito, Italy
6 Department of Physics, Florence Campus, Kent State University, Kent, OH 44240, USA
* Correspondence: simone.lolli@imaa.cnr.it; Tel.: +39-0971425250

Abstract: This study investigates changes in aerosol radiative effects on two highly urbanized regions across the Euro-Mediterranean basin with respect to a natural desert region as Sahara over a decade through space-based lidar observations. The research is based on the monthly-averaged vertically-resolved aerosol optical depth (AOD) atmospheric profiles along a $1^\circ \times 1^\circ$ horizontal grid, obtained from the Cloud-Aerosol Lidar with Orthogonal Polarization (CALIOP) instrument measurements aboard the Cloud-Aerosol lidar and Infrared Pathfinder Satellite Observation (CALIPSO). To assess the variability of the anthropogenic aerosols on climate, we compared the aerosol vertical profile observations to a one-dimensional radiative transfer model in two metropolitan climate sensible hot-spots in Europe, namely the Po Valley and Benelux, to investigate the variability of the aerosol radiative effects over ten years. The same analysis is carried out as reference on the Sahara desert region, considered subject just to natural local emission. Our findings show the efficacy of emission reduction policies implemented at government level in strongly urbanized regions. The total atmospheric column aerosol load reduction (not observed in Sahara desert region) in Po Valley and Benelux can be associated with: (i) an increase of the energy flux at the surface via direct effects confirmed also by long term surface temperature observations, (ii) a general decrease of the atmospheric column, and likely (iii) an increase in surface temperatures during a ten-year period. Summarizing, the analysis, based on the decade 2007–2016, clearly show an increase of solar irradiation under cloud-free conditions at the surface of +3.6 % and +16.6% for the Po Valley and Benelux, respectively, and a reduction of −9.0% for the Sahara Desert.

Keywords: radiative effects; radiative transfer; lidar; aerosols; CALIPSO

Citation: Landi, T.C.; Bonasoni, P.; Brunetti, M.; Campbell, J.R.; Marquis, J.W.; Di Girolamo, P.; Lolli, S. Aerosol Direct Radiative Effects under Cloud-Free Conditions over Highly-Polluted Areas in Europe and Mediterranean: A Ten-Years Analysis (2007–2016). *Remote Sens.* **2021**, *13*, 2933. https://doi.org/10.3390/rs13152933

Academic Editor: Manuel Antón

Received: 26 May 2021
Accepted: 23 July 2021
Published: 26 July 2021

1. Introduction

Europe, the so-called old continent, includes also the Western part of the Eurasia. Four times smaller than America and Asia, it hosts 11% of the World population, including some high densely populated areas. Marked by cultural diversity and origins, some of European regions are historically related to social and economical progress, e.g., the industrial revolution in the XVII century that led to an unavoidable increase in anthropogenic emissions. In the last decades, air-quality and climate related research activities identified some European regions as climate hot-spots. In these areas, resulting climate changes happen faster then respect to other areas [1–3]. Among them, we can count the Mediterranean basin, the cradle of western civilization that developed its culture and historical background with

the contribution of many diverse populations living and moving across the region, which are linked together by traditions and history. This cultural development was dramatically influenced over the last few centuries by the Mediterranean climate, which pushed local populations to develop different agricultural and farming techniques with respect to other European populations. The unique local biological heritage of this large region has a very high economic value. However, the region is also extremely sensitive to climate change [4] with some heavily industrialized areas, like the Po-Valley and Catalan region. Coastal cities also suffer relevant pollution episodes due to marine vessels [5]. On other hand, the Benelux region (Belgium, The Netherlands and Luxembourg) is considered to be another climate hotspot because it is a densely populated area, home of one of the major industrial district in Europe [6,7]. In Benelux, the recorded levels of particulate matter (PM) pollution, based on the EU's air quality standards, makes the air quality "very poor" which is the second-worst level on the air quality index, just before the "extremely poor" quality category.

The aerosol emissions in those two regions, anthropogenic and/or natural, besides deteriorating the air-quality [8], can locally warm or cool the atmospheric column, both directly through their effect in modulating incoming solar radiation and indirectly through their influence on lifetime of clouds and precipitations [9–11]. The aerosol species differently interact with incoming shortwave (SW) solar radiation and the outgoing longwave (LW) radiation emitted by the Earth surface. Shortwave reflecting aerosols, e.g., sulfates, marine aerosols, increase the planetary albedo cooling the surface [12], while black-carbon aerosol layers absorb the incoming SW radiation warming the surrounding air around them. Dust aerosol layers can either reflect the incoming SW radiation and trap the outgoing LW radiation (at a lesser extent). Both effects can alter regional atmospheric stability, vertical motions, and affect large-scale circulation and regional hydrological cycles, causing significant regional climate sensitivity [13]. The net aerosol radiative effect (RE) at ground level changed in the past few decades, especially due to anthropogenic contribution caused by the increased human industrial activities. The increase of pollutant concentrations in the atmosphere peaked in the 1970s/early 1980s followed by a substantial decrease in aerosols concentrations, resulting from mitigation policies adopted by European governments to reduce air pollution, is very likely the cause of the well documented change of surface solar radiation over the past half century known as "global dimming" (less solar radiation reaching the Earth surface), observed from the 1950s to the early 1980s. The global dimming is followed by the so-called "global brightening" (more solar radiation reaching the Earth surface) which is still happening [14,15]. Differently with respect to the global dimming, in the global brightening the clouds (which are indirectly affected by the aerosol presence) still played a dominant role on the variations of downward surface shortwave radiation (SSR) during the last few decades [16]. While the effects of greenhouse gases on climate are assessed with great accuracy, the radiative effects of the short-lived climate forcers, as those from aerosol emissions, show a much larger uncertainty. This is highlighted by the Fifth Assessment Report of the Intergovernmental Panel on Climate Change (IPCC) [17].

Surface air temperature, together with moisture, wind, and turbulent diffusion, is one of the most important meteorological parameters influencing particles dilution within the Mixing Layer Height (MLH [18]). The presence of different aerosol mixing may result in a net radiative heating/cooling of the lower atmosphere, thus promoting/inhibiting the vertical mixing and causing more/less air pollutants being transported to upper levels as a result of the increasing/decreasing the boundary layer height [19,20].

The IPCC estimates that (i) absorbing and non-absorbing aerosols have very different impacts on shortwave surface radiative cooling, and that (ii) their sizes also play a crucial role in radiative balance. A first species of fine mode aerosols are those originating from sulphates and nitrates. This kind of aerosols are non-absorbing smaller fine-mode particles that are strongly reflecting incoming solar radiation and then with a net effect of increasing the Earth-atmosphere albedo. Other fine-mode aerosol species are constituted by organic matter (e.g., organic carbon) and by strongly-absorbing soot (e.g., black carbon). Regarding

coarse-mode aerosol species, we find non-absorbing sea salt and weakly-absorbing mineral dust [21]. As a net effect, the shortwave cooling exerted by both fine and coarse-mode aerosols, e.g., sulphates, nitrates, sea salt, organic matter, and dust over oceans is on average outweighting the net warming effects by soot and dust over continents [22]. As stated by Kinne [22], if the aerosol fine-mode is mainly considered as the net anthropogenic contributor to RE, investigations of anthropogenic impacts can be limited to the cooling effect exerted by non-absorbing or weakly-absorbing species and to the warming by strongly-absorbing ones.

In quantitative terms, as stated by the latest IPCC report, the total surface anthropogenic radiative effect for 2011 relative to 1750 is +2.29 [+1.13 to +3.33] W/m^2, with a stronger acceleration starting from the 1970s compared to prior decades. The total anthropogenic RE best-estimate for 2011 is 43% higher with respect to year 2005 figures. This is caused by two combined effects: (i) continuous increase in greenhouse gas concentrations and (ii) an increase of aerosol concentrations at the surface causing a weaker net cooling effect (negative RE). Thus, atmospheric aerosol RE, which includes cloud adjustments, is overall -0.9 (-1.9 to -0.1) W/m^2 (medium confidence), which is the net result from a cooling effect from most anthropogenic aerosol species and a warming effect from black carbon solar radiation absorption.

In this study, we examine how the anthropogenic emissions influence the aerosol radiative effect at the surface in three different regions: two densely-populated European regions, i.e., Northern Italy and Benelux, and a desert region, i.e., the Bodele depression in Africa. The latter being chosen as reference because uninfluenced by human activity. Our objective is to corroborate links between atmospheric turbidity, aerosol RE at the surface and surface temperature trends. Other studies quantitatively highlighted the aerosol radiative effects over Europe [23] and their correlation with the surface temperature [24]. Nevertheless, none of these studies focused on anthropogenic aerosol emissions on regions that are critical for climate change comparing the results with a region without significant human footprints over a decade (2007–2016). In particular, this study is based on computing the trends in atmospheric turbidity and direct radiative balance at the surface, either for anthropogenic (i.e., Po Valley and Benelux, anthropogenic aerosols as black-carbon) or natural (i.e., desert area, dust) scenarios. Vertically-resolved (CALIOP, Cloud–Aerosol Lidar with Orthogonal Polarization) and columnar (AERONET, AErosol RObotic NETwork, Level 2.0) measurements of aerosols optical depth and a radiative transfer model (Fu-Liou-Gu) [25–27] are used to quantify the variability over time of the vertically-resolved profile of atmospheric aerosol load and their radiative effect. In addition, surface temperature trends (i.e., before and after the 1980), calculated for the regions of interest, are compared with atmospheric turbidity observations over a ten-year period (i.e., 2007–2016). There is high confidence that short-lived climate effects exerted by aerosols and their interactions with clouds have offset a substantial portion of global mean radiative effect from well-mixed greenhouse gases. Still, the aerosols continue to represent the largest uncertainty to total RE estimates.

2. Materials and Methods

2.1. Regions of Interest

The European Environment Agency (EEA) [28] supports implementation policies to limit regional pollutants and respect air quality standards. EU legislation contributes to the definition of air pollution policies and long-term development strategies to improve air quality in Europe. The Po-Valley and Benelux are notoriously highly-populated and industrialized areas in Europe, prone to poor surface air quality [28]. On other hand, the selected area over northern Africa (basically centered over the Bodele Depression) is recognized as one of most important sources of natural aerosols [29]. Consequently, these three different regions were used to evaluate and confirm our hypothesis of an existing link between human activities and the surface temperature variability in the Euro-Mediterranean region. We investigate trends in atmospheric turbidity over a ten-year

period and correlate aerosol radiative effect characteristics and inter-annual variability with regional surface temperatures.

2.2. Surface Air Temperature: Trend Calculation

Long-term analysis of Climate Research Unit (CRU) TS 4.02 surface temperature records derived at 0.5 latitude-longitude degree resolution by CRU [30] was produced for two periods: the first from 1951 to 1980, and the second from 1981 to 2016. The different boxes, representative of the three areas of interest (Po Valley, Benelux, and Sahara desert), are defined as shown in Figure 1. Anomalies of monthly mean temperature were calculated for the period from 2007 to 2016, the same period covered by CALIPSO measurements used for this study. Figure 2 illustrates the inter-annual anomalies relative to the ten-year mean (continuous lines), linear trends (dashed lines) computed before and after the 1980, and the period of CALIPSO observations (light-green area) considered for the comparisons reported in the Section 3.

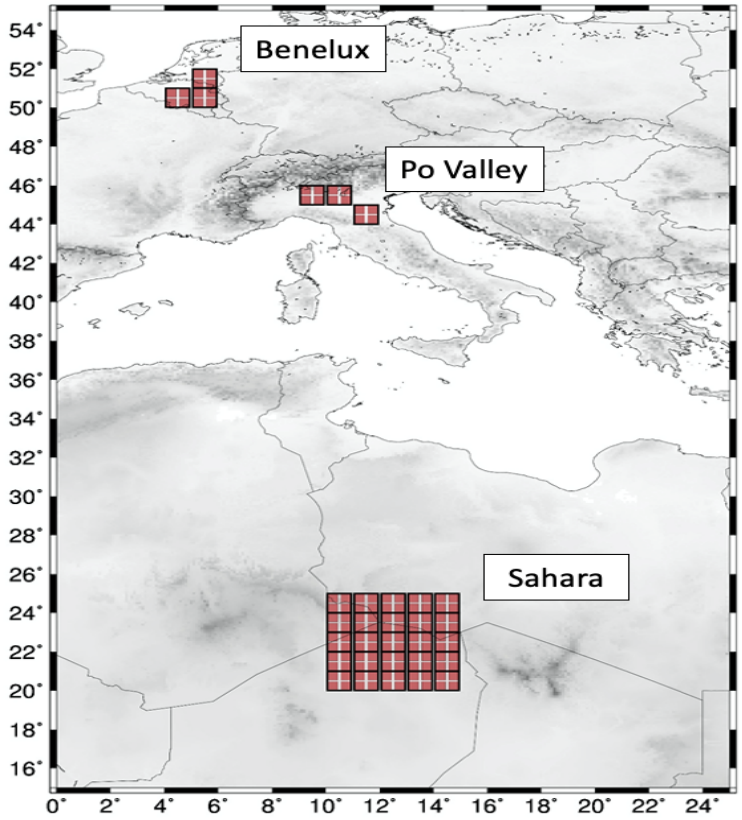

Figure 1. Regions Of Interest (ROI) considered for this study. From north to south: Benelux, Po Valley, and portions of of Sahara desert. The red boxes depict the areas considered for calculating the mean of the geophysical parameters taken into account for this study and described in the test.

The ten-year linear trend was estimated applying the Theil-Sen method [31,32] estimating its significance through the Mann-Kendall non-parametric test [33]. We split the trend calculations into two different periods—before and after the 1980—to best isolate the relatively rapid temperature increase in the last four decades. As pointed out by Figure 2, the trends have similar slopes for the most recent period. On the other hand, between 1950 and 1980, linear trends are inconsistent: the temperature behavior in the Po Valley indicates a decrease, and an increase in Benelux and desert area. This can be partially explained by the implementation of the major industrial plants in Northern Italy, e.g., automotive, steelmakers. Instead, for Benelux, the analysis needs further investigation.

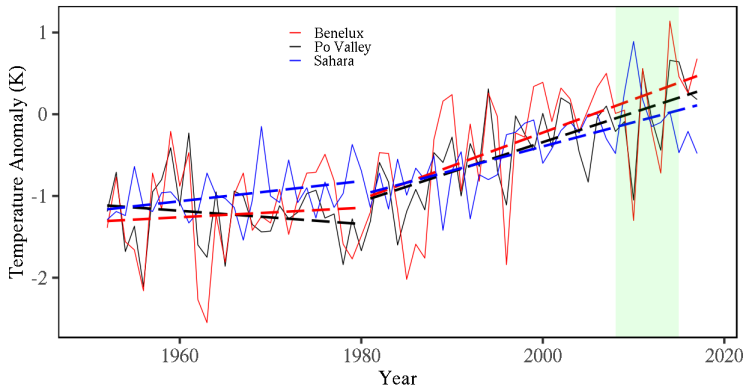

Figure 2. Time-series series of air temperature anomalies calculated over 2007–2016 period (green area). The dataset is freely available at Climate Research Unit (CRU).

2.3. Aerosol Optical Depth: CALIPSO and AERONET Measurements

The standard Cloud-Aerosol Lidar with Orthogonal Polarization (CALIOP) data products are classified by processing level according to the definitions given by NASA's Earth Observing System (EOS) project. The CALIOP Version 4.10 Level 1 data consist of profiles of attenuated backscatter coefficients at 1064 nm and 532 nm, while the Level 2 data report such quantities as layer location, layer type, and a number of derived optical parameters, including optical depths.

In this paper, we aggregate the CALIOP lidar observations of the atmospheric vertically-resolved optical depth as monthly mean profiles over a uniform spatial grid of $1^\circ \times 1^\circ$ up to an altitude of 10 km. The quality of the data is obtained through the process described by Campbell et al. [34] that replicates very closely the method described by Winker et al. [35]. The latter methodology is formally endorsed by the CALIPSO (Cloud-Aerosol Lidar and Infrared Pathfinder Satellite Observations) project team development. Nevertheless, the screening metrics in Campbell et al. [34] help to improve the retrieval method robustness for this investigation purposes. First, if the presence of a cloud is initially detected, the profile is not taken into consideration. This choice minimizes the relative attenuation of the lidar signal that can have an impact on the aerosol extinction coefficient retrieval. In the second instance, CALIOP profiles are not taken into consideration if the retrieval fails to resolve aerosol from surface up to 250 m. Lastly, based on Toth et al.'s [36] analysis, those profiles without aerosol loading (i.e., aerosol optical depth; AOD = 0) are disregarded. Applying those restrictions as a whole, it helps to limit the signal attenuation effects that could bias the averaged solutions of the aerosol extinction profiles derived for this study. An average of 1800 qualifying profiles were used each year to build the profiles used during our analysis. As final step, a Gaussian weighting function was used to solve the averages to increase the retrievals significance relative to the $1^\circ \times 1^\circ$ study domain center. Moreover, the domain-average CALIOP 532 nm aerosol extinction profiles are built with a vertical resolution of 100 m that corresponds to each of the native Level 2 species resolved for use in a radiative transfer model experiment described in Section 2.4. In Reference [34], among others, the authors characterize CALIOP AOD measurements together with their accuracy. Eventually, lidar measurements provide critical information on vertical distribution of aerosol optical properties that are especially related to air quality, climatology and climatic effects. In addition, the column-integrated aerosol optical depth derived from Level 2 CALIOP 532nm observations is also widely used in combination with passive-based L2 aerosol retrievals for a comprehensive understanding of regional and global aerosol optical properties [37].

The NASA Aerosol Robotic Network (AERONET) [38], a federated network of homogeneous commercially-available sunphotomters, has collected long-term continuous and readily accessible public domain data of aerosol optical, microphysical and radiative prop-

erties [38]. For this study, we consider the new Version 3 (V3) of Level 2 (Quality Assured) monthly AOD averages, a product directly downloadable at NASA's AERONET website.

2.4. The Fu-Liou-Gu Radiative Transfer Model

We assess the direct aerosol radiative effects using the Fu-Liou-Gu (FLG) Radiative Transfer (RT) model [19,25,26,39,40]. Following the methodology reported in Reference [41], the FLG RT code was initialized using the vertically-resolved lidar CALIPSO extinction profiles (described above) of the different aerosol species, which were matched to the Optical Properties of Aerosol and Clouds (OPAC) catalog [42]-based physical and optical models written into the code [40]. The total number of the RT model vertical levels was adjusted to match the lidar extinction spatial resolution of 100 m from ground to 10 km (100 levels). The total aerosol radiative effect is computed adding all contributions (in terms of optical depth) from the different aerosol species identified by the CALIPSO classification algorithm in the considered region and matched with the corresponding FLG aerosol species, as shown in Reference [41]. The aerosols present in the atmosphere at highly urbanized sites and desert is very different. For this reason is very important to correctly chose the different aerosol types. From CALIOP data analysis on highly urbanized sites, among the eighteen aerosol species parameterized into the FLG RT model from the OPAC catalog, we considered only the main four species that match the CALIPSO classification: transported dust (CALIPSO: "dust"), urban (CALIPSO: "polluted continental/smoke"), 50% dust, and 50% urban (CALIPSO: "polluted dust") and black carbon (CALIPSO: "smoke"). Those aerosol species account for more than 98% of the total AOD value in each region. For the Sahara desert instead, dust is the unique aerosol species present in the atmosphere. A potential source of uncertainty in parameterizing Version 4 CALIOP aerosol typing into FLG RT is that the classification algorithm cannot distinguish between local urban pollution and an advected smoke aerosol layer from distant sources below 2.5 km. Even if it is reasonable to to assume that those episodes are not frequent, they can introduce a bias in the anlysis. To compute the radiative effects at the top of the atmosphere and at the surface, the FLG RT model, which account also for aerosol hygroscopicity, solves the radiative fluxes at each level for 18 spectral bands (12 short-wave, 6 long-wave) [25,26]. For each annually averaged lidar extinction profile used as input in the FLG code, the aerosol direct radiative effect (DRE) at the bottom of the atmosphere and the vertically-resolved heating rate (HR) is computed by subtracting the net radiative flux when the aerosols are present in the atmosphere from the net radiative flux obtained with pristine conditions, as shown in Equation (1):

$$DRE, HR = FLG^{TotalSkyAerosol} - FLG^{Pristine}. \quad (1)$$

The ancillary data needed as input by the FLG model (i.e., the atmospheric thermodynamic variable profiles as the temperature, the atmospheric pressure, the mixing ratio and ozone concentration) are obtained from a mid-latitude standard atmosphere (USS976) for Po Valley and Benelux regions, while, for Sahara, we use the tropical standard atmosphere USS976 profiles, except for the relative humidity that was taken from the arctic atmosphere. The Solar Zenith Angle (SZA), used in FLG computations, is calculated for each box at noon local time of the 15th day of the month. While the anthropogenic aerosol contribution to LW radiative fluxes is negligible [19], dust aerosol layers (Sahara region) trap the outgoing longwave radiative fluxes (which strongly depend on water vapor). Nevertheless, the dust net radiative balance still remains negative at the surface. Following the approach reported in Reference [43], we applied a wavelength-independent constant albedo value of 0.12 for the two urban environments and 0.37 for the Sahara Desert (obtained integrating the hemispherical directional reflectance [44]), while the infrared surface emissivity is set to a constant value of 0.98.

3. Results and Discussion

3.1. Correlations between the Atmospheric Turbidity and Surface Air Temperature

Comparisons between long term time series of air temperature and aerosol optical depth (AOD) observations, as measured by AERONET and CALIOP, were performed to investigate trends throughout the considered period for this work (see Figure 1). CALIPSO measurements, covering the ten-year period (2007–2016), were analyzed to understand temporal variability of aerosol vertical distribution. The CALIOP lidar AOD is retrieved inverting the lidar equation (Equation (2)):

$$P_\lambda(r)r^2 = C_\lambda O_\lambda(r)[\beta_{mol}(r) + \beta_{aer}(r)]T^2_\lambda(r), \quad (2)$$

where $P_\lambda(r)r^2$ is the range corrected received power, C_λ is related to the system calibration coefficient, and $T^2_\lambda(r)$ is the total two-way signal transmission containing the integration of $\alpha_{tot}(r)$ the total extinction coefficient. $\beta_{mol}(r)$ and $\beta_{aer}(r)$ are the molecular and aerosol backscattering coefficients, respectively. The total two-way transmission can be expressed as (Equation (3))):

$$T^2_\lambda = exp^{-2*AOD}, \quad (3)$$

while the AOD is defined as (Equation (4)

$$AOD = \int_0^r \alpha_p(r')dr', \quad (4)$$

where α_{aer} is the aerosol extinction coefficient in km^{-1}, and r is the top of the atmosphere. Equation (2) has two unknowns (the extinction and backscattering aerosol coefficients) because the molecular optical properties can be retrieved using ancillary data, e.g., pressure and temperature profiles from the standard atmosphere. CALIPSO retrieval algorithm assumes a range independent ratio between the extinction and backscattering aerosol coefficient constant, the so-called lidar ratio (in *sr*):

$$S = \frac{\alpha_{aer}}{\beta_{aer}}. \quad (5)$$

S shows a very high variability (20–120 *sr*), depending on the aerosol species [45]. The used values in CALIPSO retrieval can be found in Reference [46]. The authors decided to split, by arbitrary choice, the lower troposphere into three (3) levels to investigate the inter-annual variability of the atmospheric turbidity within the mixing layer height. For this study, we consider both the total AOD, and the AOD calculated at different vertical intervals from 40 m above the ground up to 2 km as follows: level 1 from 40 m to 500 m, level 2 from 500 m to 1 km, and level 3 from 1 km to 2 km. Together with AOD and air temperature, the aerosol radiative effects at the bottom-of-the-atmosphere (BOA) were computed by using the FLG Radiative Transfer Model (see Section 2.4).

In order to provide a quantitative assessment of the behavior of such parameters on the polluted regions subject to a strong human activity, as well as in natural desert zones, trend calculations were carried out based on the monthly averages of the lidar data aggregated from the original CALIPSO Level 2 products previously described. Table 1 reports the percentage variation of the computed radiative fluxes estimated per decade of AOD and BOA during 2007–2016 as inferred by CALIPSO observations through the Sen method. According to Toth et al. [47], this method is preferable when data are noisy as its output is a nonparametric estimate of the slope after computing all points dataset median of pairwise slopes. Nevertheless, our analysis shows some limitations because data are really noisy and often the correlation is not significant ($p > 0.1$). The same analysis on temperature records (Section 2.2), which, due to the higher temporal resolution, are much less noisy is much more statistical significant. On other hand, analysis on CALIOP data still gives indication on the observed trend during the decade, confirming the negative trend shown in Europe by Toth et al. [47].

Table 1. Percentage increase/decrease (i.e., +/−) per decade of AOD and BOA radiative flux during 2007–2016 calculated on monthly mean values from CALIPSO by using the Theil-Sen slopes (de-seasonalized monthly values). Levels indicate the AOD calculated for lev1: $z_0 = 40$ m and $z_1 = 500$ m; lev2: $z_0 = 500$ m and $z_1 = 1$ km; lev3: $z_0 = 1$ km and $z_1 = 2$ km.

	% /10 Years (AOD and BOA 2007–2016)		
	Po Valley	**Benelux**	**Sahara**
Total AOD	−3.4	−16.5	+4.8
lev3 AOD	+3.9	−15.5	+8.7
lev2 AOD	−10.1	−14.0	+8.0
lev1 AOD	−14.3	−19.6	+8.5
BOA	+3.6	+16.6	−9.0

During the analyzed decade, the AOD trend and, consequently, the total atmospheric turbidity for the Po Valley and Benelux is negative (i.e., −3.4% and −16.5%, respectively), which is associated with an increase of the incoming solar irradiation at the surface under cloud-free conditions (+3.6% and +16.6%, respectively). Because more solar radiation is reaching the ground, as a consequence, a net warming effect of the surface air masses is likely.

The authors speculate that high concentrations of fine and/or absorbing particles originated from combustion processes might be one of the most important causes of surface temperature increase. In fact, highly urbanized/industrialized areas, such as Po Valley and Benelux, are characterized by important sources of black carbon [48]. It is well-known that such type of particles absorb the incoming solar radiation influencing the vertical heating rate close to the major emission sources, while, far from emission areas, it can contribute to the surface temperature increase as a diabatic heat insulator. For instance, in 2004, Johnson et al. [49] demonstrated the warming effect of absorbing particles within the mixing layer. Recently, Sand et al. [50] found a non-linear relationship between emissions rate and temperature variation at ground level: the higher is the BC emission rate, the lower is the air temperature sensitivity because the convection in the lower atmospheric levels promote convection and turbulent motion moving BC from the surface to the mixing layer top. In other words, the net motion results in enhancing aerosol upward vertical transport. Such conditions favor the pollutant dilution within the atmospheric mixing layer resulting in lower AOD values at lower levels (e.g., level 1 and level 2 of Table 1). But, on the other hand, the positive aerosol load increase above 1km found in the Po-Valley might be also ascribed to the northern Africa mineral dust transport [51]. Dust outbreaks in Po-Valley occur with a frequency that spans between 10 and 15 events per year [51]. Over the Benelux, the impact of desert mineral dust is significantly lower as it is inversely related with latitude [52]. In fact, the AOD values decrease overall in the considered layers [53]. This translates into higher solar energy reaching the surface as suggested by the FLG computed BOA. This is consistent with the more rapid air temperature increase over the considered decade in Benelux compared to Po Valley (see Figure 2).

Over the desert regions, our results highlight an increase of the total AOD. A thicker aerosol dust layer over the years causes a reduction of the solar irradiance reaching the surface. This effect is partially compensated by the outgoing longwave radiation trapped by the dust layer, but still the net balance at the surface is negative. Such analysis points out that the net solar radiation reaching the ground decreased during the last decade, but the surface air temperature (see Figure 2) increased: this net warming effect is a consequence of the greenhouse gases concentration increase over the decade.

Figure 3 illustrates the long-term temperature measurement record (1980–2020) and AOD both from space (CALIOP) and from ground measurements (AERONET; see Figure 3) for the Po Valley (upper panel), Benelux (middle), and Sahara (lower). Starting from the monthly averages, monthly air temperature deviations from the ten-year mean are also reported, coupled with the monthly averages of both CALIOP and AERONET observations.

Looking at the surface temperature behavior, we find an unequivocal increase for the three considered areas. However, this increase has different causes depending on the considered region as previously described. The temperature trends put in evidence about 0.4 degrees/10 yr increment for urbanized areas (i.e., 0.43 degrees/10 yr in Benelux and 0.37 degrees/10 yr in Po Valley) and about 0.3 degrees/10 yr (i.e., 0.28 degrees/10 yr) for the desert region .

From lidar vertically-resolved observations, it is clear how changes in human activity differently shaped the surface and vertically-resolved AOD observations during the analyzed decade in the Po Valley and Benelux with respect to the desert Bodele depression. The AOD reduction is significant for the high-urbanized areas, on the other hand, as stated above, an increase of atmospheric turbidity is observed over the desert region (see Table 1). Such discrepancies are even more evident if we consider the trend calculated from CALIOP measurements. As reported in Table 1, AOD decrement is observed in both the Po Valley (up to 1 km) and Benelux (overall the column); on the contrary, the AOD enhances (overall the column) for Sahara.

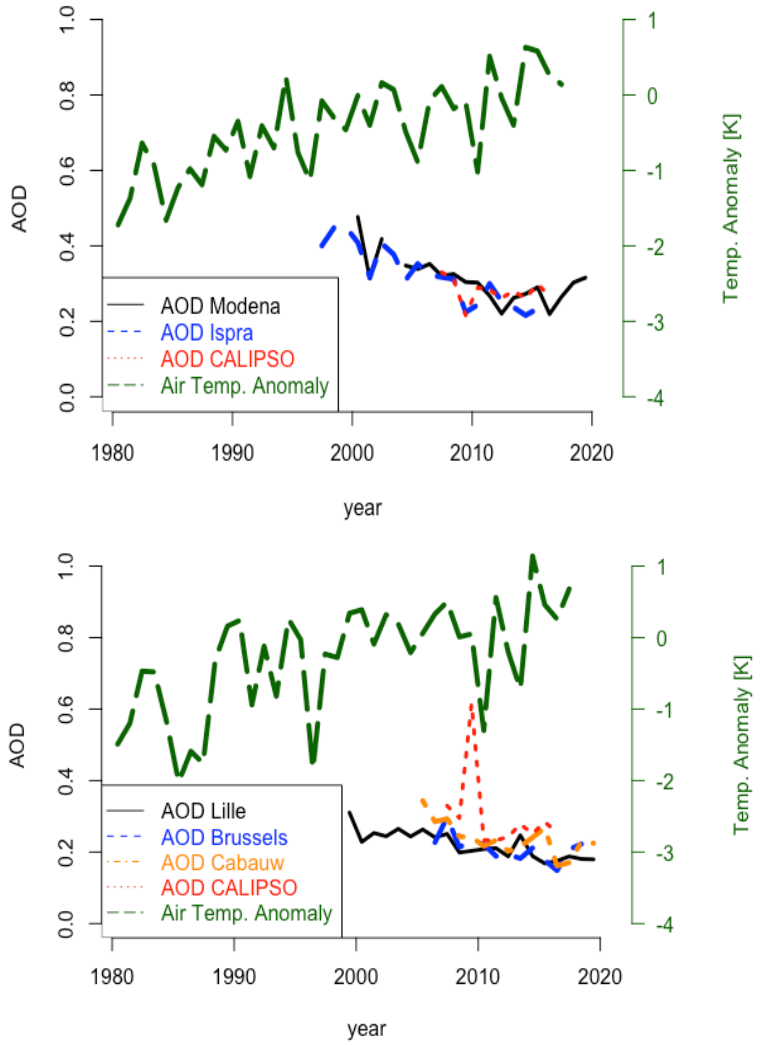

Figure 3. *Cont.*

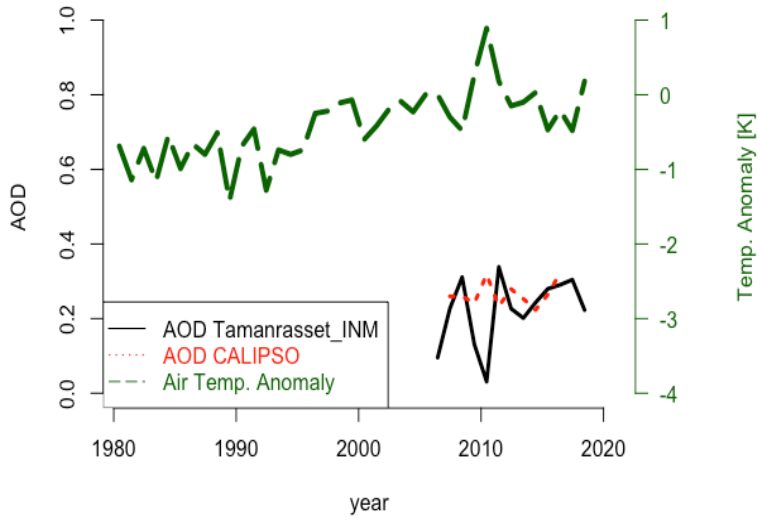

Figure 3. Time-series of aerosol optical depth (AOD) measured by AERONET permanent observing sites (Po Valley: Modena, 44.63°N, 10.94°E, Elevation 56 m; Ispra, 45.80°N, 8.63°E, Elevation 235 m; Benelux: Lille, 50.61°N, 3.14°E, Elevation: 60 m; Brussels, 50.78°N, 4.35°E, Elevation: 120 m; Cabauw, 51.97°N, 4.93°E, Elevation −1 m; Sahara: Tamanrasset INM, 22.79°N, 5.53°E, Elevation 1377 m) and from space by CALIPSO, together with the temperature anomalies computed over the 10-year period covered by satellite measurements (2007–2016). The upper panel represents the Po Valley, the middle panel represents the Benelux, and the lower panel represents the Sahara.

4. Conclusions

Through our study, we finally give quantitative evidence to the changes in direct radiative effect under cloud-free conditions associated with anthropogenic aerosol emissions over a decade (2007–2016) in two highly-urbanized Euro-Mediterranean areas, i.e., the Po-Valley in Southern Europe and the Benelux in central Europe. We compared our findings with those of a wild and remote region not affected by human activity as the Sahara Desert, taken as reference. Through this study, using interpolated surface temperature measurements and remote sensing observations of the Aerosol Optical Depth (AOD) both vertically-resolved (from lidar) and columnar (from AERONET sunphotometers), for the first time, we quantitatively assess how much the implementation of emission mitigation policies reversed the so-called "aerosol dimming" over the polluted regions.

This research was carried out taking into account long term temperature anomalies, the satellite observations of atmospheric turbidity and the calculation of direct radiative effects. In higher urbanized regions, we considered four main aerosol species (through CALIPSO lidar observations) accounting for 98% the total Aerosol Optical Depth (AOD), dust (natural source), urban (anthropogenic source), black carbon (anthropogenic source), and polluted dust (anthropogenic source). As expected, in the desert region, the aerosol is 100% dust (natural source).

The aerosol direct radiative effects were estimated through the Fu-Liou-Gu Radiative Transfer Model using the CALIOP extinction profiles as input. The analysis carried on the Po-Valley and Benelux regions highlights a reduction of aerosol concentration in the atmosphere after year 2000 that yields an increase of solar radiation at the surface, which is compatible with the observed AOD yearly reduction rate of 0.005–0.01 yr^{-1}.

Results can be summarized as follows: (i) in the Po Valley and Benelux, two highly urbanized/industrialized regions (where anthropogenic aerosols are dominant) the columnar aerosol loading and the surface air temperature trends are inversely related (i.e., consistent with a reduction in solar dimming), while (ii) in the Sahara region (where the anthropogenic pressure is absent and crustal aerosol is dominant) the atmospheric turbidity does not appear to be temporally correlated with changes in surface air temperature.

These results reveal that the aerosol loading should be taken into consideration when assessing the temporal variability of the surface radiative flux budget. In particular, the concomitant increment of atmospheric transparency, and the enhancement of atmospheric greenhouse gases concentrations, can likely be considered as the two most significant effects that promote surface temperature increase. With respect to these considerations, additional quantitative investigations are required in future experiments and studies. A further appropriate assessment of spatial-temporal variations requires deeper investigations, as suggested by the differences between the highly populated areas and desert areas pointed out by this study.

More in-depth studies are also required to investigate the real effect of the solar irradiance (i.e., +3.6% in Po Valley and +16.6% in Benelux) in increasing the air temperature at the surface, considering the concurrent effects due to the presence of absorbing and reflecting aerosol layers at higher altitudes.

Author Contributions: Conceptualization, T.C.L. and S.L.; methodology, T.C.L., M.B., S.L., P.B., P.D.G.; software, S.L, T.C.L., M.B., J.W.M., J.R.C.; validation, T.C.L., S.L., M.B., P.B., P.D.G.; formal analysis, T.C.L., M.B, P.B., P.D.G.; investigation, T.C.L., S.L., J.R.C., J.W.M., M.B., P.B., P.D.G.; resources, P.B.; data curation, M.B., J.R.C., J.M.; writing—original draft preparation, T.C.L., S.L., M.B.; writing—review and editing, P.D.G., S.L., J.R.C., P.D.G., P.B.; visualization, P.B.; supervision, P.B.; project administration, P.B., M.B.; funding acquisition, P.B. All authors have read and agreed to the published version of the manuscript

Funding: This research received no external funding.

Institutional Review Board Statement: Not applicable.

Informed Consent Statement: Not applicable.

Data Availability Statement: CALIOP data are freely available from NASA Langley Research Center, while meteorological data are freely available at Climatic Research Unit (University of West Anglia) and NCAS. The algorithms used in the analysis are developed under MATLAB and available upon request.

Acknowledgments: The authors thank Climatic Research Unit (University of East Anglia) and NCAS for providing temperature data. CALIOP data were obtained from the NASA Langley Research Center Atmospheric Science Data Center. The authors wish also to thank the three anonymous reviewers for their constructive comments. A special thank to Domenico Trotta that gave us a professional contribution in improving and editing English language and style all over the manuscript.

Conflicts of Interest: The authors declare no conflict of interest.

References

1. Nicholls, R.J.; Wong, P.P.; Burkett, V.; Woodroffe, C.D.; Hay, J. Climate change and coastal vulnerability assessment: scenarios for integrated assessment. *Sustain. Sci.* **2008**, *3*, 89–102. [CrossRef]
2. Lewis, S.C.; King, A.D.; Perkins-Kirkpatrick, S.E.; Mitchell, D.M. Regional hotspots of temperature extremes under 1.5 °C and 2 °C of global mean warming. *Weather. Clim. Extrem.* **2019**, *26*, 100233. [CrossRef]
3. Spiegl, T.; Langematz, U. Twenty-First-Century Climate Change Hot Spots in the Light of a Weakening Sun. *J. Clim.* **2020**, *33*, 3431–3447. [CrossRef]
4. Guiot, J.; Cramer, W. Climate change: The 2015 Paris Agreement thresholds and Mediterranean basin ecosystems. *Science* **2016**, *354*, 465–468. [CrossRef]
5. Mueller, D.; Uibel, S.; Takemura, M.; Klingelhoefer, D.; Groneberg, D.A. Ships, ports and particulate air pollution—An analysis of recent studies. *J. Occup. Med. Toxicol.* **2011**, *6*, 1–6. [CrossRef]
6. Harrison, P.A.; Butterfield, R.E.; Orr, J.L. Modelling climate change impacts on wheat, potato and grapevine in Europe. In *Climate Change, Climatic Variability and Agriculture in Europe*; Environmental Change Unit, University of Oxford: Oxford, UK, 2000; pp. 367–390.
7. Hinkel, J.; Nicholls, R.J.; Vafeidis, A.T.; Tol, R.S.; Avagianou, T. Assessing risk of and adaptation to sea-level rise in the European Union: An application of DIVA. *Mitig. Adapt. Strateg. Glob. Chang.* **2010**, *15*, 703–719. [CrossRef]
8. Bilal, M.; Nazeer, M.; Nichol, J.; Qiu, Z.; Wang, L.; Bleiweiss, M.P.; Shen, X.; Campbell, J.R.; Lolli, S. Evaluation of Terra-MODIS C6 and C6. 1 aerosol products against Beijing, XiangHe, and Xinglong AERONET sites in China during 2004–2014. *Remote Sens.* **2019**, *11*, 486. [CrossRef]

9. Crosier, J.; Allan, J.; Coe, H.; Bower, K.; Formenti, P.; Williams, P. Chemical composition of summertime aerosol in the Po Valley (Italy), northern Adriatic and Black Sea. *Q. J. R. Meteorol. Soc.* **2007**, *133*, 61–75. [CrossRef]
10. Stanhill, G. A perspective on global warming, dimming, and brightening. *Eos Trans. Am. Geophys. Union* **2007**, *88*, 58–58. [CrossRef]
11. Perrino, C.; Catrambone, M.; Dalla Torre, S.; Rantica, E.; Sargolini, T.; Canepari, S. Seasonal variations in the chemical composition of particulate matter: A case study in the Po Valley. Part I: Macro-components and mass closure. *Environ. Sci. Pollut. Res.* **2014**, *21*, 3999–4009. [CrossRef] [PubMed]
12. Bilal, M.; Nazeer, M.; Nichol, J.E.; Bleiweiss, M.P.; Qiu, Z.; Jäkel, E.; Campbell, J.R.; Atique, L.; Huang, X.; Lolli, S. A simplified and robust surface reflectance estimation method (SREM) for use over diverse land surfaces using multi-sensor data. *Remote Sens.* **2019**, *11*, 1344. [CrossRef]
13. Menon, S.; Hansen, J.; Nazarenko, L.; Luo, Y. Climate effects of black carbon aerosols in China and India. *Science* **2002**, *297*, 2250–2253. [CrossRef] [PubMed]
14. Wild, M. Global dimming and brightening: A review. *J. Geophys. Res. Atmos.* **2009**, *114*. [CrossRef]
15. Sanchez-Lorenzo, A.; Wild, M.; Brunetti, M.; Guijarro, J.A.; Hakuba, M.Z.; Calbó, J.; Mystakidis, S.; Bartok, B. Reassessment and update of long-term trends in downward surface shortwave radiation over Europe (1939–2012). *J. Geophys. Res. Atmos.* **2015**, *120*, 9555–9569. [CrossRef]
16. Mateos, D.; Sanchez-Lorenzo, A.; Antón, M.; Cachorro, V.E.; Calbó, J.; Costa, M.J.; Torres, B.; Wild, M. Quantifying the respective roles of aerosols and clouds in the strong brightening since the early 2000s over the Iberian Peninsula. *J. Geophys. Res. Atmos.* **2014**, *119*, 10–382. [CrossRef]
17. Stocker, T.F.; Qin, D.; Plattner, G.-K.; Tignor, M.; Allen, S.K.; Boschung, J.; Nauels, A.; Xia, Y.; Bex, V.; Midgley, P.M. (Eds.) *IPCC: Climate Change 2013: The Physical Science Basis. Contribution of Working Group I to the Fifth Assessment Report of the Intergovernmental Panel on Climate Change*; Cambridge University Press: Cambridge, UK; New York, NY, USA, 2013; p. 1535.
18. Vivone, G.; D'Amico, G.; Summa, D.; Lolli, S.; Amodeo, A.; Bortoli, D.; Pappalardo, G. Atmospheric boundary layer height estimation from aerosol lidar: A new approach based on morphological image processing techniques. *Atmos. Chem. Phys.* **2021**, *21*, 4249–4265. [CrossRef]
19. Lolli, S.; Khor, W.Y.; Matjafri, M.Z.; Lim, H.S. Monsoon Season Quantitative Assessment of Biomass Burning Clear-Sky Aerosol Radiative Effect at Surface by Ground-Based Lidar Observations in Pulau Pinang, Malaysia in 2014. *Remote Sens.* **2019**, *11*, 2660. [CrossRef]
20. Zheng, Y.; Che, H.; Xia, X.; Wang, Y.; Wang, H.; Wu, Y.; Tao, J.; Zhao, H.; An, L.; Li, L.; et al. Five-year observation of aerosol optical properties and its radiative effects to planetary boundary layer during air pollution episodes in North China: Intercomparison of a plain site and a mountainous site in Beijing. *Sci. Total. Environ.* **2019**, *674*, 140–158. [CrossRef]
21. Granados-Muñoz, M.J.; Sicard, M.; Román, R.; Benavent-Oltra, J.A.; Barragán, R.; Brogniez, G.; Denjean, C.; Mallet, M.; Formenti, P.; Torres, B.; et al. Impact of mineral dust on shortwave and longwave radiation: Evaluation of different vertically resolved parameterizations in 1-D radiative transfer computations. *Atmos. Chem. Phys.* **2019**, *19*, 523–542. [CrossRef]
22. Kinne, S. Aerosol radiative effects with MACv2. *Atmos. Chem. Phys.* **2019**. [CrossRef]
23. Norris, J.R.; Wild, M. Trends in aerosol radiative effects over Europe inferred from observed cloud cover, solar "dimming," and solar "brightening". *J. Geophys. Res. Atmos.* **2007**, *112*. [CrossRef]
24. Gettelman, A.; Shindell, D.; Lamarque, J. Impact of aerosol radiative effects on 2000–2010 surface temperatures. *Clim. Dyn.* **2015**, *45*, 2165–2179. [CrossRef]
25. Fu, Q.; Liou, K.N. On the correlated k-distribution method for radiative transfer in nonhomogeneous atmospheres. *J. Atmos. Sci* **1992**, *49*, 2139–2156. [CrossRef]
26. Fu, Q.; Liou, K.N. Parameterization of the Radiative Properties of Cirrus Clouds. *J. Atmos. Sci.* **1993**, *50*, 2008–2025. [CrossRef]
27. Lolli, S.; Campbell, J.R.; Lewis, J.R.; Gu, Y.; Welton, E.J. Fu–Liou–Gu and Corti–Peter model performance evaluation for radiative retrievals from cirrus clouds. *Atmos. Chem. Phys.* **2017**, *17*, 7025–7034. [CrossRef]
28. European Environment Agency. Air Quality in Europe—2018 Report. EEA Report 12/2018. 2018. Available online: https://www.eea.europa.eu/publications/air-quality-in-europe-2018 (accessed on 25 July 2021).
29. Todd, M.C.; Washington, R.; Martins, J.V.; Dubovik, O.; Lizcano, G.; M'bainayel, S.; Engelstaedter, S. Mineral dust emission from the Bodélé Depression, northern Chad, during BoDEx 2005. *J. Geophys. Res. Atmos.* **2007**, *112*. [CrossRef]
30. Harris, I.; Jones, P.D.; Osborn, T.J.; Lister, D.H. *Version 4 of the CRU TS Monthly High-Resolution Gridded Multivariate Climate Dataset*; Nature Publishing Group: London, UK, 2020; Volume 7, pp. 1–18.
31. Sen, P.K. Estimates of the regression coefficient based on Kendall's tau. *J. Am. Stat. Assoc.* **1968**, *63*, 1379–1389. [CrossRef]
32. Theil, H. A rank-invariant method of linear and polynomial regression analysis, 3; confidence regions for the parameters of polynomial regression equations. *Indag. Math.* **1950**, *1*, 467–482.
33. Sneyers, R. On the use of statistical analysis for the objective determination of climate change. *Meteorol. Z.* **1992**, *1*, 247–256. [CrossRef]
34. Campbell, J.; Tackett, J.; Reid, J.; Zhang, J.; Curtis, C.; Hyer, E.; Sessions, W.; Westphal, D.; Prospero, J.; Welton, E.; et al. Evaluating nighttime CALIOP 0.532 μm aerosol optical depth and extinction coefficient retrievals. *Atmos. Meas. Tech.* **2012**, *5*, 2143–2160. [CrossRef]

35. Winker, D.; Tackett, J.; Getzewich, B.; Liu, Z.; Vaughan, M.; Rogers, R. The global 3-D distribution of tropospheric aerosols as characterized by CALIOP. *Atmos. Chem. Phys.* **2013**, *13*, 3345–3361. [CrossRef]
36. Toth, T.D.; Campbell, J.R.; Reid, J.S.; Tackett, J.L.; Vaughan, M.A.; Zhang, J.; Marquis, J.W. Minimum aerosol layer detection sensitivities and their subsequent impacts on aerosol optical thickness retrievals in CALIPSO level 2 data products. *Atmos. Meas. Tech.* **2018**, *11*, 499–514. [CrossRef] [PubMed]
37. Lolli, S.; Alparone, L.; Garzelli, A.; Vivone, G. Haze Correction for Contrast-Based Multispectral Pansharpening. *IEEE Geosci. Remote Sens. Lett.* **2017**, *14*, 2255–2259. [CrossRef]
38. Holben, B.N.; Eck, T.F.; Slutsker, I.; Tanre, D.; Buis, J.; Setzer, A.; Vermote, E.; Reagan, J.A.; Kaufman, Y.; Nakajima, T.; et al. AERONET—A federated instrument network and data archive for aerosol characterization. *Remote Sens. Environ.* **1998**, *66*, 1–16. [CrossRef]
39. Gu, Y.; Farrara, J.; Liou, K.; Mechoso, C. Parameterization of cloud–radiation processes in the UCLA general circulation model. *J. Clim.* **2003**, *16*, 3357–3370. [CrossRef]
40. Gu, Y.; Liou, K.; Ou, S.; Fovell, R. Cirrus cloud simulations using WRF with improved radiation parameterization and increased vertical resolution. *J. Geophys. Res. Atmos.* **2011**, *116*. [CrossRef]
41. Tosca, M.G.; Campbell, J.; Garay, M.; Lolli, S.; Seidel, F.C.; Marquis, J.; Kalashnikova, O. Attributing accelerated summertime warming in the southeast united states to recent reductions in aerosol burden: Indications from vertically-resolved observations. *Remote Sens.* **2017**, *9*, 674. [CrossRef]
42. Hess, M.; Koepke, P.; Schult, I. Optical properties of aerosols and clouds: The software package OPAC. *Bull. Am. Meteorol. Soc.* **1998**, *79*, 831–844. [CrossRef]
43. Lolli, S.; Campbell, J.R.; Lewis, J.R.; Gu, Y.; Marquis, J.W.; Chew, B.N.; Liew, S.C.; Salinas, S.V.; Welton, E.J. Daytime Top-of-the-Atmosphere Cirrus Cloud Radiative Forcing Properties at Singapore. *J. Appl. Meteorol. Climatol.* **2017**, *56*, 1249–1257. [CrossRef]
44. Strahler, A.H.; Muller, J.; Lucht, W.; Schaaf, C.; Tsang, T.; Gao, F.; Li, X.; Lewis, P.; Barnsley, M.J. MODIS BRDF/albedo product: Algorithm theoretical basis document version 5.0. *Modis Doc.* **1999**, *23*, 42–47.
45. Lolli, S.; Di Girolamo, P. Principal component analysis approach to evaluate instrument performances in developing a cost-effective reliable instrument network for atmospheric measurements. *J. Atmos. Ocean. Technol.* **2015**, *32*, 1642–1649. [CrossRef]
46. Kim, M.H.; Omar, A.H.; Tackett, J.L.; Vaughan, M.A.; Winker, D.M.; Trepte, C.R.; Hu, Y.; Liu, Z.; Poole, L.R.; Pitts, M.C.; et al. The CALIPSO version 4 automated aerosol classification and lidar ratio selection algorithm. *Atmos. Meas. Tech.* **2018**, *11*, 6107–6135. [CrossRef]
47. Toth, T.D.; Zhang, J.; Campbell, J.R.; Reid, J.S.; Vaughan, M.A. Temporal variability of aerosol optical thickness vertical distribution observed from CALIOP. *J. Geophys. Res. Atmos.* **2016**, *121*, 9117–9139. [CrossRef]
48. Mukherjee, A.; Agrawal, M. World air particulate matter: sources, distribution and health effects. *Environ. Chem. Lett.* **2017**, *15*, 283–309. [CrossRef]
49. Johnson, B.; Shine, K.; Forster, P. The semi-direct aerosol effect: Impact of absorbing aerosols on marine stratocumulus. *Q. J. R. Meteorol. Soc.* **2004**, *130*, 1407–1422. [CrossRef]
50. Sand, M.; Berntsen, T.K.; Ekman, A.M.; Hansson, H.C.; Lewinschal, A. Surface temperature response to regional black carbon emissions: Do location and magnitude matter? *Atmos. Chem. Phys.* **2020**, *20*, 3079–3089. [CrossRef]
51. Duchi, R.; Cristofanelli, P.; Landi, T.C.; Arduini, J.; Bonafe, U.; Bourcier, L.; Busetto, M.; Calzolari, F.; Marinoni, A.; Putero, D.; et al. Long-term (2002–2012) investigation of Saharan dust transport events at Mt. Cimone GAW global station, Italy (2165 m asl) Long-term investigation of Saharan dust transport events at Mt. Cimone. *ELementa Sci. Anthr.* **2016**, *4*, 85. [CrossRef]
52. Pey, J.; Querol, X.; Alastuey, A.; Forastiere, F.; Stafoggia, M. African dust outbreaks over the Mediterranean Basin during 2001–2011: PM10 concentrations, phenomenology and trends, and its relation with synoptic and mesoscale meteorology. *Atmos. Chem. Phys.* **2013**, *13*, 1395. [CrossRef]
53. Mehta, M.; Singh, R.; Singh, A.; Singh, N.; Anshumali. Recent global aerosol optical depth variations and trends—A comparative study using MODIS and MISR level 3 datasets. *Remote Sens. Environ.* **2016**, *181*, 137–150. [CrossRef]